⁶Lower-Tropospheric Eddy Momentum Fluxes in Idealized Models and Reanalysis Data

NICHOLAS J. LUTSKO

Program in Atmospheric and Oceanic Sciences, Princeton University, Princeton, New Jersey

ISAAC M. HELD

NOAA/Geophysical Fluid Dynamics Laboratory, Princeton, New Jersey

PABLO ZURITA-GOTOR

Instituto de Geociencias, Universidad Complutense de Madrid, Madrid, Spain

AMANDA K. O'ROURKE

Department of Earth and Environmental Sciences, University of Michigan, Ann Arbor, Michigan

(Manuscript received 3 April 2017, in final form 5 September 2017)

ABSTRACT

In Earth's atmosphere eddy momentum fluxes (EMFs) are largest in the upper troposphere, but EMFs in the lower troposphere, although modest in amplitude, have an intriguing structure. To document this structure, the EMFs in the lower tropospheres of a two-layer quasigeostrophic model, a primitive equation model, and the Southern Hemisphere of a reanalysis dataset are investigated. The lower-tropospheric EMFs are very similar in the cores of the jets in both models and the reanalysis data, with EMF divergence (opposing the upper-tropospheric convergence) due to relatively long waves with slow eastward phase speeds and EMF divergence (as in the upper troposphere) due to shorter waves with faster eastward phase speeds.

As the two-layer model is able to capture the EMF divergence by long waves, a qualitative picture of the underlying dynamics is proposed that relies on the negative potential vorticity gradient in the lower layer of the model. Eddies excited by baroclinic instability mix efficiently through a wide region in the lower layer, centered on the latitude of maximum westerlies and encompassing the lower-layer critical latitudes. Near these critical latitudes, the mixing is enhanced, resulting in increased EMF convergence, with compensating EMF divergence in the center of the jet. The EMF convergence at faster phase speeds is due to deep eddies that propagate on the upper-tropospheric potential vorticity gradient.

1. Introduction

One of the distinctive features of Earth's troposphere is the convergence of angular momentum in mid-latitudes by large-scale eddies. This transfer mainly takes place in the upper troposphere, where the convergence of eddy momentum flux (EMF) helps sustain an eddy-driven jet in each hemisphere. From a wavemean flow perspective, the conventional explanation for

Oenotes content that is immediately available upon publication as open access.

Corresponding author: Nicholas Lutsko, lutsko@princeton.edu

this pattern in the EMF is that baroclinic zones in midlatitudes act as source regions for eddies, which propagate meridionally until they break near their critical latitudes (Randel and Held 1991). The irreversible process of breaking transfers momentum from the sink regions, where the waves break, to the source regions, where the eddies originate (e.g., Held 1975; Vallis 2006).

As EMFs are much larger in the upper troposphere than in the lower troposphere, there has been little study of lower-tropospheric EMFs. However, O'Rourke and Vallis (2016) recently showed that in an idealized dry GCM, long-wavelength eddies with slow eastward propagation *diverge* momentum away from the eddy-driven jet in the lower troposphere in Earth-like settings. While these fluxes are weak and do not contribute

substantially to the vertically integrated flux that controls the near-surface winds, Chai et al. (2016) found that the EMFs in the lower troposphere of a similar idealized, dry GCM grow in magnitude when the frictional damping time scale near the surface is increased, reaching values comparable to the upper-level EMFs when this time scale is increased by several orders of magnitude (a parameter setting that may be relevant for studying Jupiter's atmosphere). The long, slow waves responsible for these lower-tropospheric EMFs may also play a more prominent role in double-jet states (Kim and Lee 2004; O'Rourke and Vallis 2013) and in superrotating atmospheres (Saravanan 1993).

Here, we study the EMFs in the lower troposphere of two different idealized models and in a reanalysis dataset. We start by comparing the EMFs in the upper and lower troposphere of the reanalysis data. Next, we ask whether the idealized models can reproduce the features seen in the reanalysis data and then use the models to interpret this behavior of the eddies. The models we use are a two-layer quasigeostrophic (QG) model on a β plane and a dry primitive-equation model, which we will refer to as the GCM. The two-layer QG model formed the basis for the first numerical study of the general circulation (Phillips 1956) and has continued to play an important role in the theoretical development of atmospheric dynamics, being used for instance by some of the authors of the present paper in studies of baroclinic wave packets (Lee and Held 1993), in the development of eddy closure schemes (Pavan and Held 1996; Held and Larichev 1996; Zurita-Gotor 2007), in idealized studies of annular modes (Zurita-Gotor et al. 2014; Zurita-Gotor 2014), and in tests of the fluctuationdissipation theorem (Lutsko et al. 2015). The value of the two-layer QG model in these studies is that, despite its simplicity, it is able to capture many key features of the observed dynamics of the midlatitude troposphere. In this study, we use it as the base of a model hierarchy for studying lower-tropospheric EMFs. The GCM is used to test how the two-layer dynamics carry over into the more complex setting of a primitive equation model on a sphere, providing a connection from the two-layer model to the reanalysis dataset.

2. Data, models, and methods

a. Reanalysis data

The observational data are taken from the Modern-Era Retrospective Analysis for Research and Applications (MERRA) dataset (Rienecker et al. 2011). To make as clean a comparison as possible with the idealized models, only data from the Southern Hemisphere

have been used and we focus on austral summer [December–March (DJFM)]. As discussed in section 3, the main features we are interested in are present in all seasons but are seen most clearly in austral summer.

b. Two-layer QG model

The two-layer QG model is the same as in Lutsko et al. (2015). It consists of two different density layers on a β plane in which the meridional temperature gradient (i.e., the slope of the interface) is relaxed toward an equilibrium profile. The layers have equal depths, and bottom friction is present in the lower layer. In nondimensional form, the equations are

$$\begin{split} \frac{\partial q_k}{\partial t} + J(\psi_k, q_k) &= -\frac{1}{\tau_d} (-1)^k (\psi_1 - \psi_2 - \psi_R) \\ &- \frac{1}{\tau_f} \delta_{k2} \nabla^2 \psi_k - \nu \nabla^4 q_k, \end{split} \tag{1}$$

where $q_k = \nabla^2 \psi_k + (-1)^k (\psi_1 - \psi_2) + \beta y$ is the potential vorticity (PV) in the upper (k = 1) and lower (k = 2) layers, the ψ_k s are the corresponding streamfunctions, τ_d is a Newtonian relaxation time scale, τ_f is a Rayleigh friction time scale acting only in the lower layer (this is indicated by the Kronecker δ function), and ν is a hyperdiffusion coefficient.

The model domain is a zonally periodic channel with a baroclinic zone in the center of the domain created by setting the radiative equilibrium temperature $(\psi_1 - \psi_2)$ gradient to a hyperbolic secant centered at y=0. In radiative equilibrium (i.e., in the absence of eddy fluxes), the lower layer flow ψ_2 is identically zero so that the zonal flow in the upper layer $U_1(y) = -\partial \psi_1/\partial y = -\partial \psi_R/\partial y$ is

$$-\frac{\partial \psi_R}{\partial y} = \operatorname{sech}^2(y/\sigma), \qquad (2)$$

where σ sets the half-width of the jet.

The maximum strength of the vertical shear of the zonal wind in radiative equilibrium is being used as the velocity scale U in nondimensionalizing these equations, while the length scale L is the deformation radius. The time scale is then L/U, which we refer to as a "model day," although it is only about a fifth of a day for plausible choices of L and U. We prefer to describe results from the two-layer model nondimensionally because there is no unambiguously optimal choice of parameters that provides the best comparison with observations.

The control nondimensional parameter settings are $\beta = 0.2$, $\sigma = 3.5$, $\tau_f = 15$, $\tau_d = 100$, and $\nu = 0.01$. The code is spectral in both x and y, and the streamfunctions are periodic in y as well, so an easterly jet is forced to exist at

the boundaries, with the same half-width and strength as the westerly jet in the center of the domain. Sponges prevent eddies from growing on this jet on the boundaries. This is the same scheme as used, for example, by Lee and Held (1993) and Lutsko et al. (2015). We use a wide domain, with zonal length $L_x = 46$ and meridional width $L_v = 68$, to ensure that the sponges do not affect the dynamics of the jet in the center of the channel. These parameter settings are nondimensionalized versions of those used by Zurita-Gotor et al. (2014), who showed that they produce an Earth-like climate. For instance, in observations, the ratio of eddy kinetic energy to zonal-mean kinetic energy is approximately unity on Earth, and this is often a good measure of realistic Earth-like nonlinearity in an idealized model. This ratio is a reasonable value of 1.3 in the two-layer model when these parameters are used.

Each simulation was run for 10000 model days, with data recorded once every 4 model days; 42 and 85 zonal and meridional Fourier modes are retained, respectively, using a standard spectral transform algorithm that computes the projection of nonlinear products onto the retained modes exactly. We have conducted a variety of parameter variations to test for robustness, but the most interesting, discussed in section 5, is the sensitivity of the EMFs to the strength of the frictional damping.

A potentially important difference with Earth's atmosphere is that the jet is not "self maintaining" in this setup. Following Robinson (2006), a jet is self-maintaining if there is a maximum in the upper-level PV flux (i.e., since the flux is negative, a minimum in the amplitude of the flux) in the core of the jet. This means that eddies break near their critical latitudes, so the baroclinicity is reduced more on the flanks of the jet than in the center and is what is observed in Earth's jets. Eddies in the two-layer model typically break well before reaching their critical latitudes (Lee 2010), so in this sense, the EMFs in the model are quite different from those in Earth's atmosphere. Weak baroclinic instability (high β) and strong friction are required to produce a self-maintaining jet in the two-layer model (Pavan and Held 1996; Lee 2010), so it is difficult to produce a climate that is both Earth-like in its energy levels and has a self-maintaining jet.

c. Primitive-equation model

The idealized atmospheric GCM is the GFDL spectral dynamical core, which solves the primitive equations for a dry ideal gas and is forced by zonally symmetric Newtonian relaxation to a prescribed equilibrium temperature field and damped by Rayleigh friction near the surface. The standard Held and Suarez (1994) parameter settings were used. The model was run at T85 resolution with 30 vertical levels for 10 000 days,

with the first 500 days discarded as spinup and data recorded once per day. The stratosphere is poorly represented in this model.

d. Methods

For both the GCM and the reanalysis data, we use 300 hPa as a representative upper-tropospheric level and 800 hPa as a representative lower-tropospheric level. The choice of lower-tropospheric level is more significant in the reanalysis data than in the idealized GCM because topography intrudes into this level in the reanalysis data. We have discarded all data for which this is the case and linearly interpolate across these grid points. The lowest level at which this does not qualitatively affect the results in the vicinity of the jet is 800 hPa. However, intruding topography is particularly an issue at high latitudes, so we have cut off our analysis of the lower-tropospheric spectra at 65°S. At lower latitudes, the majority of the data are retained, but there are still some discontinuities, mainly due to the Andes. Since the Andes mostly sit between about 30° and 10°S, they do not affect the spectra near the jet significantly.

Our main analysis tool is eddy flux cospectra, as used by Hayashi (1971), Randel and Held (1991), and many others. We follow the same procedure as Randel and Held (1991). First, u and v are transformed from (time, longitude) space to (frequency, wavenumber) space at each latitude by taking the 2D Fourier transforms. The spectra are then smoothed in frequency space using a normalized Gaussian filter of the form

$$W(\omega - \omega_0) = e^{-[(\omega - \omega_0)/\Delta\omega]^2}, \qquad (3)$$

where ω is frequency and we use $\Delta\omega=4\pi$ inverse time units. Next, the cross-power spectral density of the transformed u and v are estimated using Welch's method with eight nonoverlapping windows to give the space–time cospectra of (u,v) at each latitude. Finally, we interpolate the spectra to (phase speed, wavenumber) space for the two-layer model or (angular phase speed \times a, wavenumber) space for the GCM and reanalysis data, where a is Earth's radius. On the sphere, it is the angular phase speed rather than the phase speed that is conserved by Rossby wave packets. Finally, we sum over all wavenumbers to obtain the spectra as functions of (angular) phase speed and latitude. Seasonal spectra are estimated by calculating the spectra for each year individually and then averaging over all years (35 in total).

3. EMFs in reanalysis data

The average DJFM EMF divergence in the Southern Hemisphere of the reanalysis dataset is shown in the left

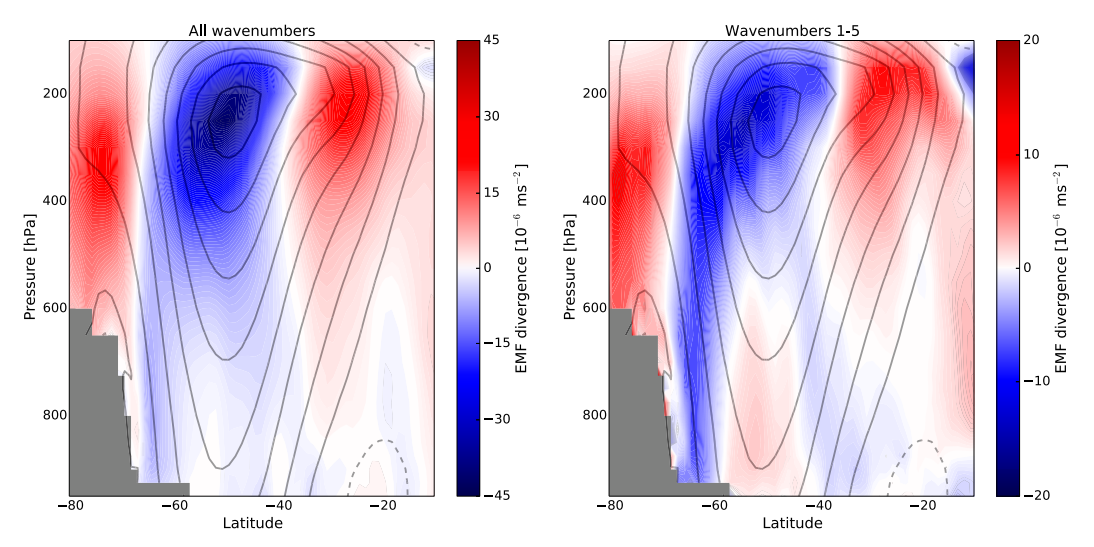


FIG. 1. (left) The average DJFM EMF divergence in the Southern Hemisphere of the MERRA data (color) and the zonal-mean zonal winds (gray contours every 4 m s⁻¹; negative values dashed). Locations at which topography intrudes into more than one-third of the grid points are shaded. (right) The contribution of eddies with wavenumbers 1–5 to the total average DJFM EMF divergence. Note the different scales of the color bars.

panel of Fig. 1 for reference. There is a region of strong EMF convergence close to the maximum jet speed, centered at about 250 hPa and 50°S, and on either side of this convergence are regions of weaker EMF divergence, with more divergence on the equatorward side of the jet than on the poleward side. The maximum EMF divergence on the poleward side of the jet is at a lower altitude (~350 hPa) than the equatorward maximum. As discussed in the introduction, the EMFs are much larger in the upper than in the lower troposphere.

The right panel of Fig. 1 shows the contribution of eddies with wavenumbers 1–5 to the average EMF divergence in this season. The pattern is generally quite similar to that of the total EMF divergence; however, in the lower troposphere, there is a region of EMF divergence in the jet core centered at about 850 hPa. There are regions of EMF convergence on either side of this, with the convergence on the poleward side being particularly strong. As in the idealized model of O'Rourke and Vallis (2016) then, long waves transfer momentum out of the jet in the lower troposphere.

The top panels of Figs. 2 and 3 show the divergence of the DJFM EMF cospectra at the 300- and 800-hPa levels, respectively. The upper-tropospheric fluxes are familiar, with EMF convergence in midlatitudes and EMF divergence in the subtropics near the eddies' critical latitudes. There is also some divergence near the poleward critical latitudes. The eddies mostly propagate eastward with angular phase speeds of 5–20 m s⁻¹, and the maximum convergence takes place in the jet core at an angular phase speed of approximately 15 m s⁻¹.

In the lower troposphere, there is EMF divergence at slow ($\leq 10 \,\mathrm{m\,s^{-1}}$) phase speeds in the center of the jet. This divergence at slow phase speeds is seen in all seasons but is most prominent in DJFM, which is why we focus on austral summer here. Equatorward of this divergence is a region of EMF convergence near the flank of the jet in the lower troposphere, where lower-tropospheric eddies would be expected to break. There appears to be strong EMF convergence on the poleward side of the jet in the lower troposphere; this is expected from Fig. 1 but could equally be due to contamination by the intruding topography. There is also a region of weak EMF convergence in the jet center at phase speeds close to the maximum lower-tropospheric jet speed ($\sim 20 \,\mathrm{m\,s}^{-1}$) and a region of EMF divergence in the subtropics at phase speeds close to the subtropical jet speed in the upper troposphere.

The middle and bottom panels of Figs. 2 and 3 show the spectra calculated using only zonal wavenumbers 1–5 and using only wavenumbers 6 and greater, respectively. In the upper troposphere (Fig. 2), the spectra are quite similar in these two spectral ranges, though wavenumbers 6 and higher contribute more to the EMF convergence in the center of the jet. The EMF by the high zonal wavenumbers is strongly biased toward the equator, whereas that due to the smaller wavenumbers is fairly symmetric about the center of the jet.

In the lower troposphere, the low-wavenumber eddies are responsible for the EMF divergence in the jet center, as well as the EMF convergence on the flanks of the jet (Fig. 3). The pattern of the high-wavenumber eddies is similar to what is seen in the upper troposphere, as there

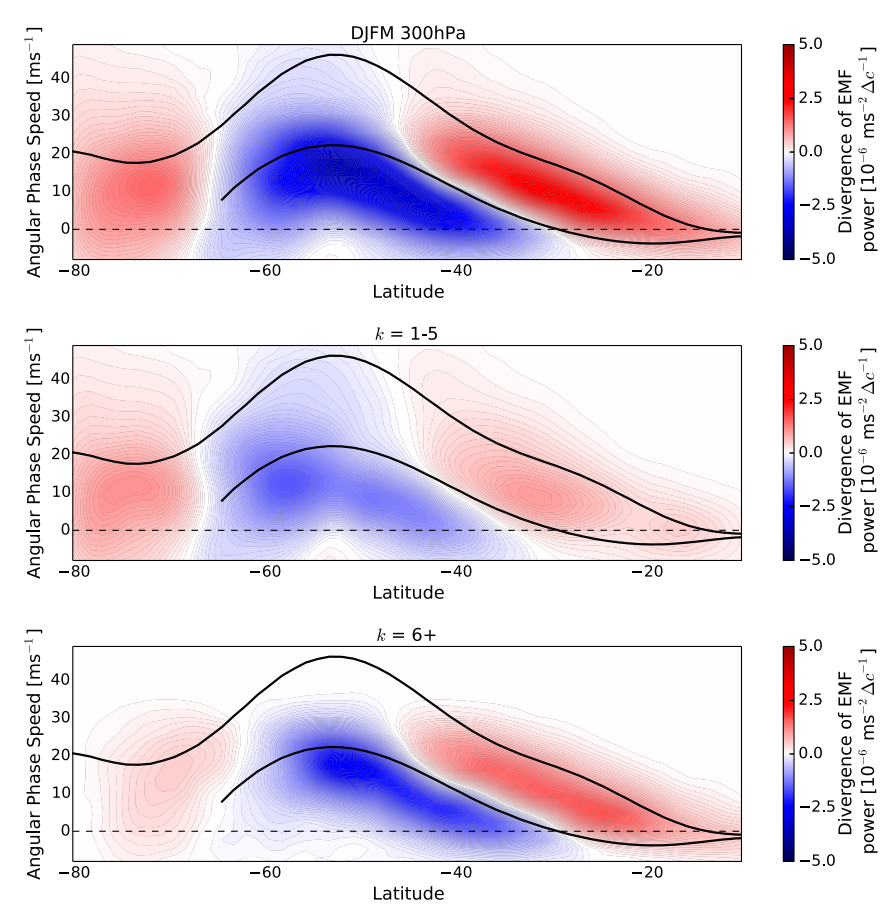


FIG. 2. (top) DJFM average of the divergence of the EMF cospectra at the 300-hPa level in the MERRA data. (middle) As in (top), but with the cospectra only calculated using wavenumbers 1–5. (bottom) As in (top), but with the cospectra only calculated using wavenumbers 6 and higher. The black curves show the zonal-mean zonal winds at 300 and 800 hPa; $\Delta c = 2.3 \, \text{m s}^{-1}$.

is EMF convergence at fast phase speeds in the jet center and EMF divergence in the subtropics; the EMF convergence by these waves cancels out the divergence by the low-wavenumber eddies somewhat.

This distinction between the high-wavenumber eddies, which are similar in the upper and lower troposphere, and the low-wavenumber eddies, which behave differently in the upper and lower troposphere, is what we will focus on with the idealized models.

4. EMF spectra of the idealized models

Figure 4 shows the divergence of the EMF cospectra in the lower troposphere of the idealized models. As before, the top panels show the spectra calculated using all wavenumbers, the middle panels show the spectra calculated using wavenumbers 1–5, and the bottom panels show the contributions from higher wavenumbers. Panels in the left column show results from the QG model, and panels in the right column show results from the GCM.

The upper-tropospheric spectra of both models have been studied by many others in the past, so we do not show them here (e.g., Lee 1997; Chen et al. 2007; Kidston et al. 2011; O'Rourke and Vallis 2016).

In the lower layer of the QG model, there is a dipole in the center of the domain, with a maximum in the EMF convergence at phase speeds close to the maximum lowerlayer wind speed and a weaker maximum in the EMF divergence at phase speeds slightly greater than zero (topleft panel of Fig. 4). The former is flanked by regions of divergence, and the latter is bordered by regions of convergence, after which there is divergence still farther from the jet. The EMF divergence in the jet center at slow phase speeds is due to low-wavenumber eddies and is partially canceled out by the EMF convergence due to shorter waves. The pattern due to the short waves resembles the pattern in the upper layer (not shown), though the EMF convergence maximum is at a faster phase speed in the lower layer. This is because there are some more slowly propagating waves that cause

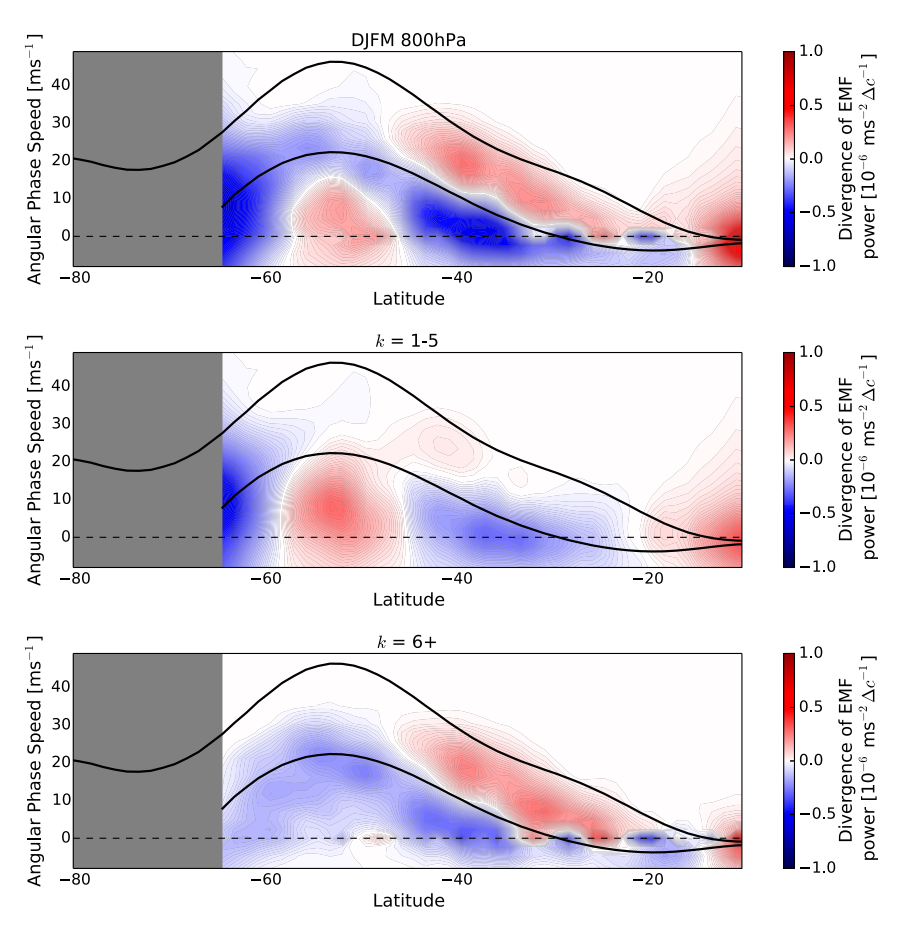


FIG. 3. As in Fig. 2, but for the 800-hPa level.

divergence in the lower layer, as the long waves do, and cancel out some of the convergence at lower phase speeds.

The lower troposphere of the GCM is similar (right column of Fig. 4), with a region of EMF convergence at fast phase speeds in the center of the jet bordered by regions of divergence and a region of EMF divergence in the center of the jet at slow phase speeds bordered by regions of convergence. The EMF divergence in the center of the jet is relatively stronger than in the QG model, though it is still weaker than the convergence. There is little evidence of the eddies being stronger on the equatorward side of the jet. Once again, the low-wavenumber eddies cause the EMF divergence in the center of the jet, and this is partially canceled out by EMF convergence due to the fast eddies. However, there is some EMF divergence at slow phase speeds by eddies with wavenumber 6, so the separation between the fast waves, which converge momentum into the jet, and the slow waves, which diverge momentum out of the jet, takes place at wavenumbers 6 and 7 in the GCM rather than at wavenumbers 5 and 6, as in the QG model and in the reanalysis data.

The lack of equatorward bias in the lower troposphere of the GCM can partly be explained by the fact that the

lower-layer winds are fairly symmetric about the jet center. The eddy heat flux (EHF), which we take as a proxy for the baroclinic stirring that excites the eddies, is also symmetric about the jet (not shown), so eddies that feel the lower-tropospheric PV gradient are equally likely to propagate poleward or equatorward.

Further insight into the behavior of the eddies can be obtained by examining zonal wavenumber–phase speed EMF cospectra at individual latitudes (rather than the divergence of these cospectra). Figure 5 shows this for the 800-hPa level in the GCM at 48°S, which is slightly poleward of the maximum jet speed. There is a clear separation between wavenumbers \leq 6, which transport momentum away from the jet at slow phase speeds, and the higher wavenumbers, which transport momentum into the jet at faster phase speeds. Note, however, that low-wavenumber eddies do transport momentum into the jet at fast (15 m s⁻¹ and higher) phase speeds, but this flux is weaker than the flux at slow phase speeds.

To understand more systematically which wavenumbers dominate the EMFs, the EMF convergence at the latitude of maximum wind speed in the upper troposphere and the EMF divergence at the latitude of maximum

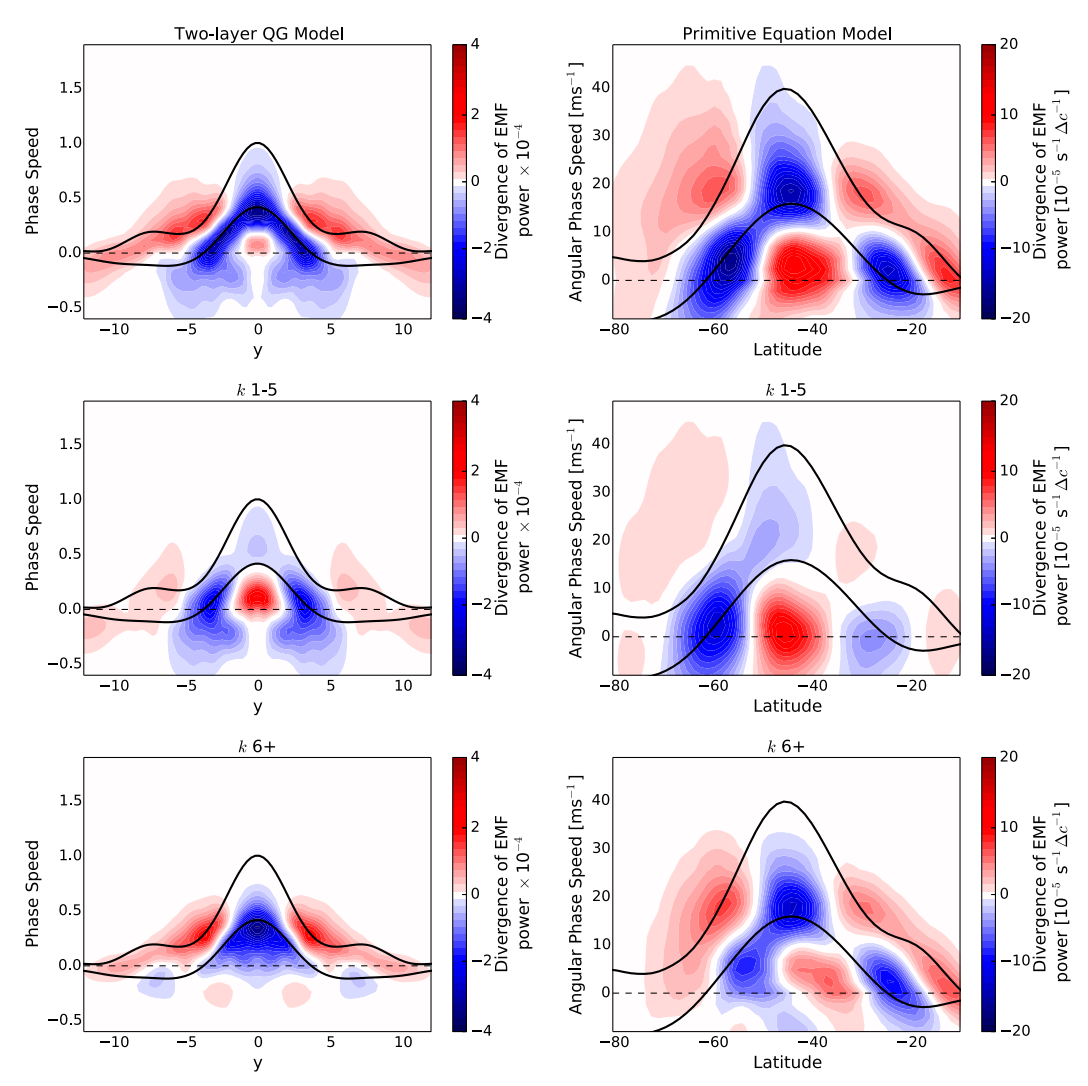


FIG. 4. As in Fig. 2, but for (left) the lower layer of the two-layer QG model and (right) the 800-hPa level in the primitive-equation model; $\Delta c = 0.06 \, \mathrm{m \, s^{-1}}$ for the QG model and $\Delta c = 2.3 \, \mathrm{m \, s^{-1}}$ for the primitive-equation model.

wind speed in the lower troposphere are plotted as a function of wavenumber for both models and for the reanalysis data in the top and middle panels of Fig. 6. The curves are normalized by their largest absolute value to facilitate comparison between the two models and the reanalysis data.

In the upper layer of the QG model, there is significant EMF convergence for wavenumbers 4 and 5, after which the EMF convergence essentially decreases with increasing wavenumber. In the GCM, the largest convergence is at wavenumbers 7 and 8. In the reanalysis data, the EMF convergence peaks at wavenumber 6 and then decreases with increasing wavenumber.

The curves for the lower layers of the two models are similar to each other, with the largest EMF divergence in the center of the domain at wavenumber 5, as was seen by O'Rourke and Vallis (2013), though wavenumbers

3 and 4 are also responsible for some EMF divergence. In the primitive equation model, there is some additional divergence due to wavenumber-6 eddies, as expected from Figs. 4 and 5. Wavenumber-4 eddies are responsible for the most EMF divergence in the reanalysis data, but wavenumber-5 eddies contribute nearly as much to the total divergence.

The differences in the EMF divergence between the two models and the reanalysis data can partly be explained by differences in the stirring. This can be seen from the bottom panel of Fig. 6, which is similar to the top and middle panels, but instead of taking the maximum of each EMF cospectrum, the integral of each EHF cospectrum is computed, giving the total EHF at each wavenumber. In agreement with the EMF results, the EHF by wavenumber 6 is much stronger in the GCM than in the QG model or in the MERRA data, while in the

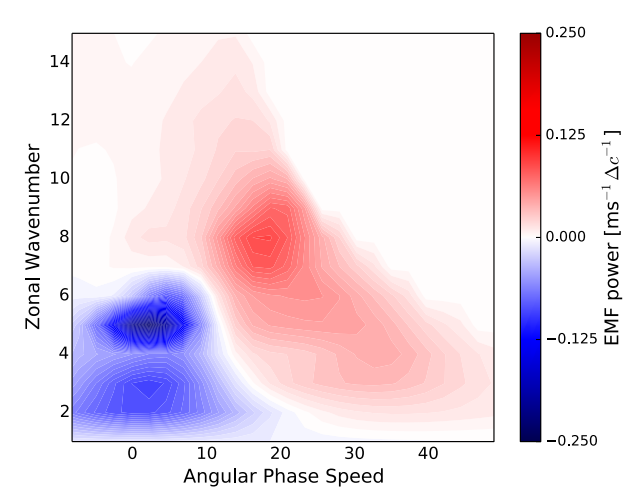


FIG. 5. Zonal wavenumber–phase speed cospectra for the eddy momentum flux at 800 hPa in the GCM at 48°S; $\Delta c = 2.3 \,\mathrm{m\,s}^{-1}$.

reanalysis data, the EHF by wavenumber 4 is stronger. There is also significant EHF by wavenumbers 7, 8, and 9 in the GCM, just as there is much EMF convergence in the upper layer of the GCM at these wavenumbers.

These comparisons show that the idealized models can reproduce many of the features of the reanalysis cospectra, though there are some differences in the relative magnitudes of the EMF divergence and convergence, as well as in the wavenumbers of the dominant eddies. Hence, it seems reasonable to interpret the reanalysis data by considering the behavior of the eddies in the idealized models. Note that the dominant wavenumbers in the QG model can be changed by adjusting the length of the channel or by varying the frictional time scale. For instance, the red curves in Fig. 6 show that if τ_F is decreased to 20 model days, the wavenumber dependence of the EMFs and the EHF in the QG model is very similar to what is seen in the MERRA data, though the zonal winds are unrealistically strong in this setup (not shown).

5. Effects of varying the frictional time scale

In a QG system, the vertically integrated EMFs must go to zero in the limit of vanishing surface friction; that is, the upper- and lower-tropospheric EMFs must cancel if they are nonzero. This implies that the lower-tropospheric EMFs must increasingly diverge momentum away from the jet and must also become stronger relative to the upper-tropospheric EMFs as friction is decreased. As mentioned in the introduction, Chai et al. (2016) found that the EMFs in the lower troposphere of an idealized GCM become much stronger and diverge momentum out of the jet when the frictional time scale is increased by several orders of magnitude relative to the standard Held–Suarez value. However, in the GCM the

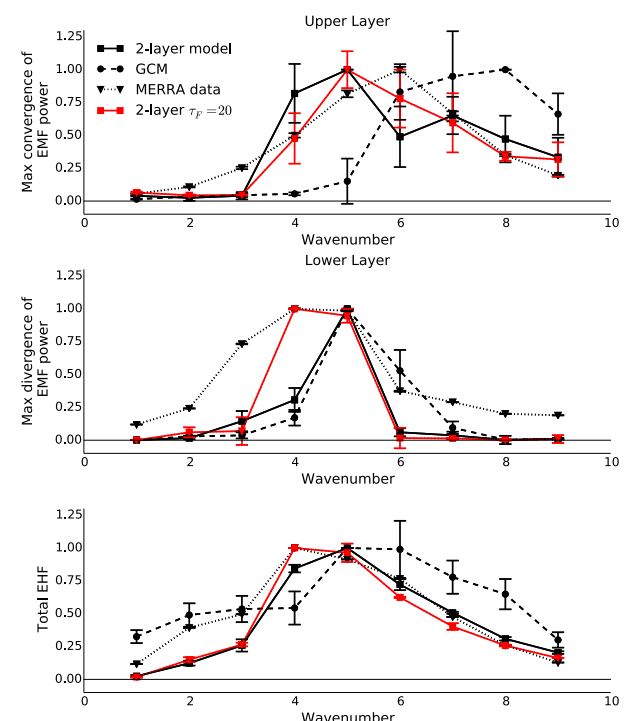


FIG. 6. (top) EMF convergence in the jet core as a function of wavenumbers 1-9 for the upper layer of the two-layer QG model (squares; black is for $\tau_F = 15$ model days, and red is for $\tau_F = 20$ model days), the 300-hPa level in the primitive-equation model (circles), and the 300-hPa level in the Southern Hemisphere of the MERRA data (triangles). The values have been normalized so that the largest absolute value of the EMF convergence is one. The error bars for the QG model and for the GCM show the spread in the values when the calculations are repeated using only the first and only the second halves of the simulations. The error bars for the MERRA data represent the standard deviations when the fluxes are calculated for each of the 35 years individually. (middle) As in (top), but for the EMF divergence in the lower layer of the two-layer QG model, the 800-hPa level in the primitive-equation model, and the 800-hPa level of the MERRA data. (bottom) The total EHF as a function of wavenumber in the lower layer of the QG model, the 800-hPa level in the primitive-equation model, and the 800-hPa level of the MERRA data.

approach to this limit is nonmonotonic, as varying friction also causes the jets to shift in latitude, which affects the propagation of eddies. For instance, there is less EMF divergence in the lower troposphere of the GCM if the frictional time scale is either doubled or halved than with the original parameter setting (not shown). It is possible to vary the surface friction in this GCM without modifying the mean winds by adding an external momentum forcing (Chen and Plumb 2009), but this is an avenue for investigating the lower-tropospheric EMF dynamics in the idealized GCM that we have not pursued.

The effects of varying friction can be studied more cleanly in the two-layer model as the position of the jet is fixed. Figure 7 plots the ratio of the lower-layer EMF divergence at y = 0 to the upper-layer EMF divergence at

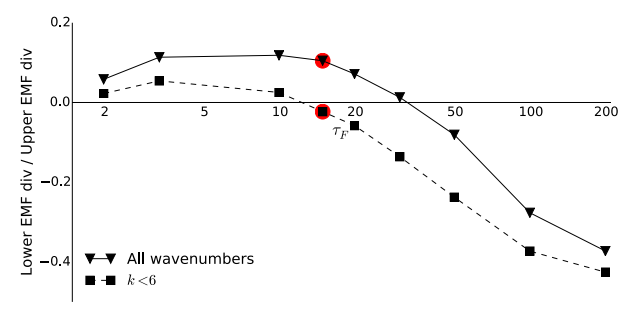


FIG. 7. The ratio of the lower-layer EMF divergence at y=0 in the QG model to the upper-layer EMF divergence at y=0 in the QG model vs the frictional time scale τ_F (solid line and triangles). The dashed line and squares show the same quantity, but only the lower-layer EMF divergence due to eddies with wavenumbers 1–5 is used. The red dots show the ratios for the control simulation.

y=0 as the frictional time scale τ_F is varied from 2.5 to 200 model days (which is roughly equivalent to two diabatic time scales). When the time scale is decreased from the control value ($\tau_F=15$ model days; red dot in the figure), the ratio initially increases slightly and then gradually decreases. Conversely, the ratio decreases and then changes sign when τ_F is increased. This decrease is roughly exponential between $\tau_F=15$ and $\tau_F=100$ model days, but then the ratio decreases more slowly between $\tau_F=100$ and $\tau_F=200$ model days.

The dashed curve in Fig. 7 shows that the decreasing ratio is because the low-wavenumber eddies increasingly diverge momentum out of the jet as τ_F is increased, while the higher-wavenumber eddies are relatively insensitive to the strength of the friction.

The EMF cospectra in both layers for the experiment with $\tau_F = 100$ model days are shown in Fig. 8. The region of EMF divergence in the lower layer is now much broader and stronger, and there is little EMF convergence in the center of the lower layer. There is also weaker divergence on the jet flanks at higher phase speeds. The pattern of the upper-layer cospectra is fairly similar to what is seen in the control run but, surprisingly, the phase speeds are relatively unchanged despite the large acceleration of the winds in both layers.

6. Interpreting the lower-tropospheric spectra

The previous sections have shown that there is a marked difference between the behaviors of the high-wavenumber (≥6) eddies and the low-wavenumber eddies in both models, as well as in the reanalysis data. The high-wavenumber eddies cause EMF convergence at fast phase speeds in the center of the jet and EMF divergence on the flanks throughout the troposphere. They also show more of an equatorward bias when spherical geometry is included. Conversely, the low-wavenumber eddies diverge momentum out of the jet in the lower

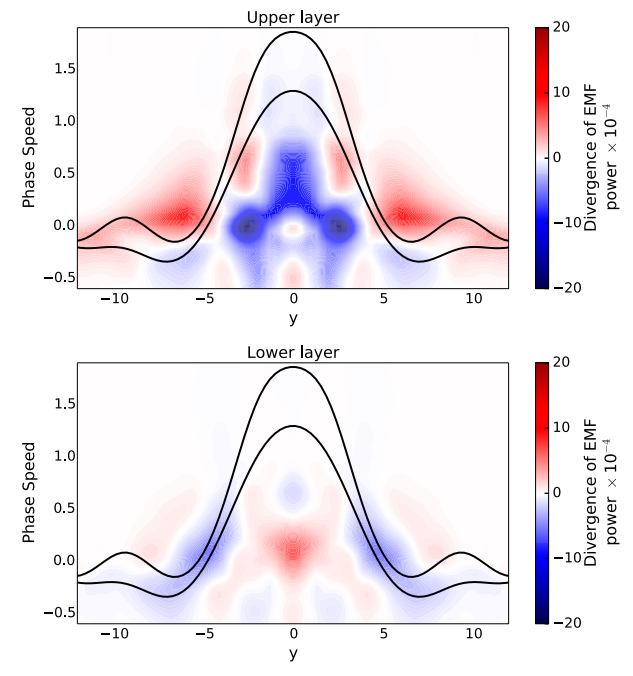


FIG. 8. Divergence of the EMF cospectra in the (top) upper and (bottom) lower layer of the two-layer QG model for the experiment with $\tau_F=100$ days. The solid black lines show the zonal-mean winds, with the upper-layer winds always being faster than the lower-layer winds; $\Delta c=0.06$.

troposphere. So understanding the lower-tropospheric cospectra requires understanding the fast, deep eddies as well as the slow eddies whose fluxes are more prominent in the lower troposphere.

The similarities of the cospectra suggest that the QG model can be used to interpret the dynamics of the lower troposphere. However, we have not been able as yet to construct a satisfying simple picture of these fluxes. From the perspective of the two-layer model, the key distinction between the lower and upper layers is the reversal in the sign of the potential vorticity gradient in the lower layer (dashed line in Fig. 9). This reversal is presumably essential to the convergence of the EMF near the lower-layer critical latitudes and divergence of the EMF at the jet center in the lower layer. But the waves responsible for this divergence propagate westward with respect to the mean winds, which is not consistent with the simplest picture of Rossby wave propagation within the lower layer on a reversed PV gradient.

A possible picture is suggested by the fact that the eddy heat flux, which we think of as the "stirring," or the source of the wave action whose horizontal rearrangement is associated with the EMF distribution, is broad enough to cover the lower-layer critical layers of the long, slow waves (contours in Fig. 9). This contrasts with the upper layer, where more propagation from the stirred

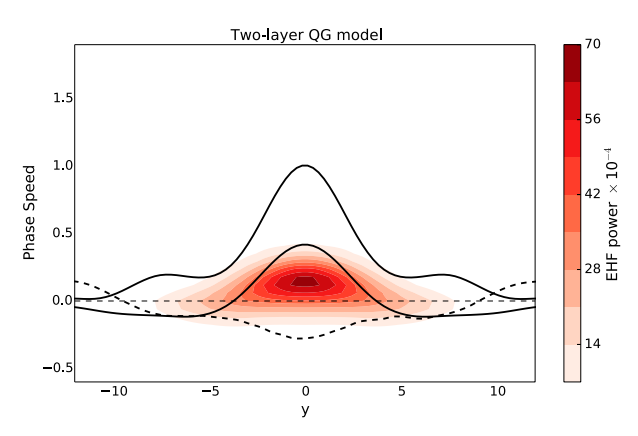


FIG. 9. Contours show the eddy heat flux cospectra in the lower layer of the two-layer QG model. The solid lines show the upper- and lower-layer zonal-mean zonal winds, and the thick dashed line shows the lower-layer PV gradient; $\Delta c = 0.06$.

region is needed to reach the critical layers for the waves dominating the EMF. So the mixing associated with waves in the lower layer can potentially be thought of as produced by the shearing and breaking of disturbances that are generated more or less in place. To the extent that this mixing is maximized near critical latitudes, the reversed sign of the PV gradient ensures that there will be EMF divergence near these critical latitudes and compensating convergence in the jet center.

We have also found that the divergent EMFs in the lower layer are very intermittent in the QG model, suggesting that a quantitative theory for these fluxes requires the characterization of rare, rather than typical, events.

In contrast, the fast eddies conform to the conventional picture of midlatitude eddy dynamics described in the introduction. These eddies are excited by baroclinic stirring, propagate meridionally away from the baroclinic zone, and then break near upper-layer critical latitudes. Because these eddies mostly propagate on the upper-layer PV gradient, they decelerate the flow where they break and accelerate the flow where they form. Although most of this momentum transfer takes place in the upper layer, there is a nonnegligible lower-layer component.

7. Conclusions

In this study we have investigated the eddy momentum fluxes in the lower troposphere of a two-layer QG model, a dry primitive-equation model, and the Southern Hemisphere of a reanalysis dataset. The EMF cospectra are very similar in the two models, showing a dipole structure in the center of the jet, with EMF convergence at phase speeds close to the lower-layer jet speed and EMF divergence at slower phase speeds. These regions are bordered by regions of EMF divergence and EMF convergence, respectively. Calculating the spectra as a

function of wavenumber shows that long, slow waves are responsible for the EMF divergence, while short, fast waves are mostly responsible for the EMF convergence at the center of the jet. Earlier studies (e.g., Hoskins et al. 1983; Blackmon et al. 1984; Feldstein 1998; Feldstein and Lee 1998; Lorenz and Hartmann 2001) also found that long-wave momentum fluxes decelerate midlatitude jets and synoptic eddies accelerate jets. However, our results are novel in that we have focused on the dynamics of the lower troposphere, which have not been studied before. Many of the same features are seen in the cospectra of the reanalysis data, particularly in austral summer, suggesting that the same fundamental dynamics are at play in the models as well as in the reanalysis data.

We suggest that the EMF divergence in the lower troposphere is due to eddies that are excited by the baroclinic stirring and that are most affected by the weak, negative PV gradient there. These eddies are well mixed over a broad region that encompasses the lower-tropospheric critical latitudes, where the mixing is enhanced, leading to EMF convergence there. In the center of the jet, there is compensating EMF divergence. The EMF convergence at faster phase speeds is due to fast, deep eddies that propagate away from the stirring region on the upper-tropospheric PV gradient. These eddies are responsible for the EMF convergence in the center of the jet in the upper troposphere but also cause significant EMF convergence in the lower troposphere.

One of the motivations for this study was the result of Chai et al. (2016) that the eddies in the lower troposphere of an idealized GCM diverge momentum when the frictional time scale is very large. This agrees with the intuition that the vertically integrated EMFs must cancel in the limit of zero surface friction. We have investigated the approach to this limit using the QG model, in which there are no complications due to jet shifts. In these simulations, the lower-layer EMF divergence increases as the frictional time scale is increased, with the increased divergence being due to the long waves.

Because of the fact that the time-mean momentum fluxes in the lower layer are a small residual of fluxes that, at any instant of time, vary over a large range of positive and negative values, as well as the strong coupling between the layers, we have not attempted to develop a quantitative theory for the parameter dependence of the lower-tropospheric EMF divergence. However, our qualitative interpretation implies that this dependence is closely tied to the nonlinear baroclinic stirring that excites the eddies. [Note that as in Ait-Chaalal and Schneider (2015), a simulation with the two-layer model in which nonlinear eddy-eddy interactions were turned off produced a very different EMF structure.] Developing a quantitative theory for this stirring and the resultant

mixing of potential vorticity is beyond the scope of this study; however, we suggest that the stochastic approach of Farrell and Ioannou (1995), DelSole (2001), and others may be a promising route to such a theory.

Acknowledgments. We thank Steve Garner and Pu Lin for helpful comments on an earlier draft of this manuscript and three anonymous reviewers for thorough readings of the manuscript. Nicholas Lutsko was supported by NSF Grant DGE 1148900 and Pablo Zurita-Gotor thanks the Cooperative Institute for Climate Science at Princeton University for support during summer 2016.

REFERENCES

- Ait-Chaalal, F., and T. Schneider, 2015: Why eddy momentum fluxes are concentrated in the upper troposphere. *J. Atmos. Sci.*, **72**, 1585–1604, doi:10.1175/JAS-D-14-0243.1.
- Blackmon, M. L., Y. H. Lee, and J. M. Wallace, 1984: Horizontal structure of 500 mb height fluctuations with long, intermediate and short time scales. *J. Atmos. Sci.*, **41**, 961–979, doi:10.1175/1520-0469(1984)041<0961:HSOMHF>2.0.CO;2.
- Chai, J., M. Jansen, and G. K. Vallis, 2016: Equilibration of a baroclinic planetary atmosphere toward the limit of vanishing bottom friction. J. Atmos. Sci., 73, 3249–3272, doi:10.1175/JAS-D-15-0329.1.
- Chen, G., and R. A. Plumb, 2009: Sensitivity of the latitude of the surface westerlies to surface friction. J. Atmos. Sci., 66, 3707–3720, doi:10.1175/2009JAS3165.1.
- —, I. M. Held, and W. A. Robinson, 2007: Sensitivity of the latitude of the surface westerlies to surface friction. *J. Atmos.* Sci., 64, 2899–2915, doi:10.1175/JAS3995.1.
- DelSole, T., 2001: A simple model for transient eddy momentum fluxes in the upper troposphere. *J. Atmos. Sci.*, **58**, 3019–3035, doi:10.1175/1520-0469(2001)058<3019:ASMFTE>2.0.CO;2.
- Farrell, B. F., and P. J. Ioannou, 1995: Stochastic dynamics of the midlatitude atmospheric jet. J. Atmos. Sci., 52, 1642–1656, doi:10.1175/1520-0469(1995)052<1642:SDOTMA>2.0.CO;2.
- Feldstein, S. B., 1998: An observational study of the intraseasonal poleward propagation of zonal mean flow anomalies. *J. Atmos. Sci.*, **55**, 2516–2529, doi:10.1175/1520-0469(1998)055<2516: AOSOTI>2.0.CO;2.
- —, and S. Lee, 1998: Is the atmospheric zonal index driven by an eddy feedback? J. Atmos. Sci., 55, 3077–3086, doi:10.1175/ 1520-0469(1998)055<3077:ITAZID>2.0.CO;2.
- Hayashi, Y., 1971: A generalized method of resolving disturbances into progressive and retrogressive waves by space Fourier and time cross-spectral analyses. J. Meteor. Soc. Japan, 49, 125–128, doi:10.2151/jmsj1965.49.2_125.
- Held, I. M., 1975: Momentum transport by quasi-geostrophic eddies. *J. Atmos. Sci.*, **32**, 1494–1497, doi:10.1175/1520-0469 (1975)032<1494:MTBQGE>2.0.CO;2.
- —, and M. J. Suarez, 1994: A proposal for the intercomparison of the dynamical cores of atmospheric general circulation models. *Bull. Amer. Meteor. Soc.*, 75, 1825–1830, doi:10.1175/ 1520-0477(1994)075<1825:APFTIO>2.0.CO;2.
- —, and V. D. Larichev, 1996: A scaling theory for horizontally homogeneous, baroclinically unstable flow on a beta plane. *J. Atmos. Sci.*, 53, 946–952, doi:10.1175/1520-0469(1996)053<0946: ASTFHH>2.0.CO;2.
- Hoskins, B. J., I. N. James, and G. H. White, 1983: The shape, propagation and mean-flow interaction of large-scale weather

- systems. J. Atmos. Sci., **40**, 1595–1612, doi:10.1175/1520-0469 (1983)040<1595;TSPAMF>2.0.CO:2.
- Kidston, J., G. K. Vallis, S. M. Dean, and J. A. Renwick, 2011: Can the increase in the eddy length scale under global warming cause the poleward shift of the jet streams? *J. Climate*, **24**, 3764–3780, doi:10.1175/2010JCLI3738.1.
- Kim, H.-K., and S. Lee, 2004: The wave–zonal mean flow interaction in the Southern Hemisphere. *J. Atmos. Sci.*, **61**, 1055–1067, doi:10.1175/1520-0469(2004)061<1055:TWMFII>2.0.CO;2.
- Lee, S., 1997: Maintenance of multiple jets in a baroclinic flow. J. Atmos. Sci., 54, 1726–1738, doi:10.1175/1520-0469(1997)054<1726: MOMJIA>2.0.CO;2.
- —, 2010: Finite-amplitude equilibration of baroclinic waves on a jet. J. Atmos. Sci., 67, 434–451, doi:10.1175/2009JAS3201.1.
- —, and I. M. Held, 1993: Baroclinic wave packets in models and observations. J. Atmos. Sci., 50, 1413–1428, doi:10.1175/1520-0469(1993)050<1413:BWPIMA>2.0.CO;2.
- Lorenz, D. J., and D. L. Hartmann, 2001: Eddy–zonal flow feedback in the Southern Hemisphere. *J. Atmos. Sci.*, **58**, 3312–3327, doi:10.1175/1520-0469(2001)058<3312:EZFFIT>2.0.CO;2.
- Lutsko, N. J., I. M. Held, and P. Zurita-Gotor, 2015: Applying the fluctuation–dissipation theorem to a two-layer model of quasi-geostrophic turbulence. *J. Atmos. Sci.*, 72, 3161–3177, doi:10.1175/JAS-D-14-0356.1.
- O'Rourke, A. K., and G. K. Vallis, 2013: Jet interaction and the influence of a minimum phase speed bound on the propagation of eddies. *J. Atmos. Sci.*, **70**, 2614–2628, doi:10.1175/JAS-D-12-0303.1.
- —, and —, 2016: Meridional Rossby wave generation and propagation in the maintenance of the wintertime tropospheric double jet. *J. Atmos. Sci.*, **73**, 2179–2201, doi:10.1175/JAS-D-15-0197.1.
- Pavan, V., and I. M. Held, 1996: The diffusive approximation for eddy fluxes in baroclinically unstable jets. *J. Atmos. Sci.*, **53**, 1262–1272, doi:10.1175/1520-0469(1996)053<1262: TDAFEF>2.0.CO;2.
- Phillips, N., 1956: The general circulation of the atmosphere: A numerical experiment. *Quart. J. Roy. Meteor. Soc.*, **82**, 123–164, doi:10.1002/qj.49708235202.
- Randel, W. J., and I. M. Held, 1991: Phase speed spectra of transient eddy fluxes and critical layer absorption. *J. Atmos. Sci.*, **48**, 688–697, doi:10.1175/1520-0469(1991)048<0688: PSSOTE>2.0.CO;2.
- Rienecker, M. M., and Coauthors, 2011: MERRA: NASA's Modern-Era Retrospective Analysis for Research and Applications. *J. Climate*, **24**, 3624–3648, doi:10.1175/JCLI-D-11-00015.1.
- Robinson, W. A., 2006: On the self-maintenance of midlatitude jets. *J. Atmos. Sci.*, **63**, 2109–2122, doi:10.1175/JAS3732.1.
- Saravanan, R., 1993: Equatorial superrotation and maintenance of the general circulation in two-level models. *J. Atmos. Sci.*, **50**, 1211–1227, doi:10.1175/1520-0469(1993)050<1211:ESAMOT>2.0.CO;2.
- Vallis, G. K., 2006: *Atmospheric and Oceanic Fluid Dynamics*. 1st ed. Cambridge University Press, 745 pp.
- Zurita-Gotor, P., 2007: The relation between baroclinic adjustment and turbulent diffusion in the two-layer model. *J. Atmos. Sci.*, **64**, 1284–1300, doi:10.1175/JAS3886.1.
- ——, 2014: On the sensitivity of zonal-index persistence to friction. J. Atmos. Sci., 71, 3788–3800, doi:10.1175/JAS-D-14-0067.1.
- —, J. Blanco-Fuentes, and E. P. Gerber, 2014: The impact of baroclinic eddy feedback on the persistence of jet variability in the two-layer model. *J. Atmos. Sci.*, 71, 410–429, doi:10.1175/ JAS-D-13-0102.1.